

Spin-dependent Schottky barriers and vacancy-induced spin-selective

Ohmic contacts in magnetic vdW heterostructures

Hongxing Li,^{a,b} Yuan-Kai Xu,^{a,b} Zi-Peng Cheng,^{a,b} Bin-Guang He,^{a,b} and Wei-Bing Zhang^{*a,b}

a School of Physics and Electronic Sciences, Changsha University of Science and Technology, Changsha 410114, People's Republic of China

b Hunan Provincial Key Laboratory of Flexible Electronic Materials Genome Engineering, Changsha University of Science and Technology, Changsha 410114, People's Republic of China

Email: zhangwb@csust.edu.cn

Abstract

The 2D ferromagnets, such as CrX₃ (X=Cl, Br and I), have been attracting extensive attentions since they provide novel platforms to fundamental physics and device applications. Integrating CrX₃ with other electrodes and substrates is an essential step to their device realization. Therefore, it is important to understand the interfacial properties between CrX₃ and other 2D materials. As an illustrative example, we have investigated the heterostructures between CrX₃ and graphene (CrX₃/Gr) from first-principles. We find unique Schottky contacts type with strongly spin-dependent barriers in CrX₃/Gr. This can be understood by synergistic effects between the exchange splitting of semiconductor band of CrX₃ and interlayer charge transfer. The spin-asymmetry of Schottky barriers may result in different tunneling rates of spin-up and down electrons, and then lead to spin-polarized current, namely spin-filter (SF) effect. Moreover, by introducing X vacancy into CrX₃/Gr, an Ohmic contact forms in spin-up direction. It may enhance the transport of spin-up electrons, and improve SF effect. Our systematic study reveals the unique interfacial properties of CrX₃/Gr, and provides a theoretical view to the understanding and designing of spintronics device based on magnetic vdW heterostructures.

Introduction

The intrinsic 2D ferromagnetic materials are the long-sought goals for both the fundamental physics and device application. According to Mermin-Wagner theorem, the long-range magnetic order is destroyed by thermal fluctuation at finite temperature.[1] However, this restriction can be eliminated by magnetic anisotropy. In 2017, the single layer CrI₃ was exfoliated successfully and proved to be an intrinsic Ising ferromagnet.[2] The discovery of CrI₃ intrigues extensive research on 2D magnets. Since then, a lot of 2D magnets have been discovered, and many novel properties have been revealed. For example, CrI₃ was proved to be a bosonic Dirac material,³ and novel electron tunneling phenomenon has been found in CrBr₃.^[4]

Magnetic tunnel junction (MTJ) is one of the most important spintronic device. Generally, one form of MTJ is the heterostructure composed by

metal/ferromagnet/insulator/ferromagnet/metal, where the ferromagnetic, insulator and metal layer are spin-filter (SF), tunneling barrier and electrode, respectively.[5] By switching the interlayer magnetic alignment, such as from antiparallel to parallel, different tunnel resistances will be obtained, namely magnetoresistance effect. Unfortunately, the number of materials that can be used to design MTJs is limited,[6] and the higher magnetoresistance (MR) is desired at present.[7] The emergence of 2D ferromagnetic materials and magnetic vdW heterostructures stacking by various 2D materials revolutionize the MTJ.[8] Comparing with the traditional MTJs, the atomic flat interface in vdW heterostructures can render uniform tunneling, which may result in higher MR. In addition, the interlayer space can serve as natural tunneling barriers.

The electrode is another key component in the MTJs-based electronic devices. Among various 2D electrode candidates, graphene is one of most widely used material due to its high-performance and low-cost. For example, the graphene has been used in CrX₃-based spin device including the multiple-spin-filter MTJs,[4,9-15] and very high large tunneling MR values up to 19 000% has been reported. Furthermore, as vacancy is inevitable in 2D materials, which is known to affect the physical properties of host remarkably. Therefore, it is crucial to understand the properties of interface between CrX₃ and graphene, and explore the effect of defect on the properties of CrX₃/Gr heterostructures.

In present paper, by first-principles calculations, we systematically study the electronic and interfacial properties of CrX₃/Gr vdW heterostructures. We find that the Schottky contacts form at the interface. Distinct from ordinary semiconductor-metal interface, the Schottky barriers Φ exhibits strong spin-dependence. Specially in the case of CrI₃/Gr, the Schottky barriers for electron Φ_e in spin-up direction is 30 meV, but up to 760 meV in spin-down. This interesting phenomenon will lead to different tunneling rates of spin-up and spin-down electrons, and the SF effect. In addition, we find the X vacancy induces interesting defect bands into the spin-up channel of CrX₃. Furthermore, in CrX₃/Gr with X vacancy (CrX₃@X_v), the Fermi level crosses the spin-up band of CrX₃ layer, which leads to Ohmic contact in spin-up direction, and possibly enhance the SF effect.

Results and discussions

Single-layer CrX₃

As presented in Figure 1, the Cr atoms in single-layer CrX₃ arrange in one plane, forming a honeycomb lattice. Each Cr atom is surrounded by six nearest neighbor X atoms that arranged in an octahedra. Due to the octahedral crystal field, the d orbit splits into low-energy t_{2g} and high-energy e_g orbit. At the same time, the X atoms provide superexchange path between Cr atoms, which are responsible for the long range ferromagnetic order,[16] and even the out-plane anisotropy.[17] The optimized in-plane lattice constants of CrX₃ are 6.10 (CrCl₃), 6.35 (CrBr₃) and 7.01 Å (CrI₃), due to the increasing of halogen atomic radii. The lattice constant of graphene is optimized to be

2.45 Å. These results agree well with the reported values.[18-20] In our study, the supercell of CrCl₃/Gr, CrBr₃/Gr and CrI₃/Gr used in calculation are composed by 2×2 CrCl₃, 2×2 CrBr₃ and $\sqrt{3} \times \sqrt{3}$ CrI₃ and 5×5 graphene, with total 74, 74 and 68 atoms, respectively. As the stiffness of graphene is larger than CrX₃, we keep graphene unstrained. The lattice mismatches lead to 0.4%, 3.4% and 1.0% strain in CrCl₃, CrBr₃ and CrI₃, respectively.

Figure 2(a)-(c) depict the spin-polarized band structures of single-layer CrX₃. We can see that these compounds are half-semiconductors with gaps of 1.58, 1.36 and 1.11 eV for CrCl₃, CrBr₃ and CrI₃, respectively. The decreasing trend of band gap from CrCl₃ to CrI₃ is in line with the crystal field strength from Cl to I. More interestingly, the band structures also show strong spin polarization. For instance, the conduction band minimum (CBM) of CrBr₃ in spin-up and spin-down direction are about 1.09 eV and 1.63 eV. We further calculate the band structures of defective CrX₃. The defective CrX₃ are modeled by removing a X atom from lattice matched CrX₃/Gr heterostructures. The corresponding atomic vacancy concentrations are 4.2%, 4.2% and 5.6% for CrCl₃, CrBr₃ and CrI₃, respectively. The band structures are shown in 2(d)-(f). Comparing with pristine CrX₃ layer, the most obvious difference is the emergence of defect bands in gap region, which are resulted from the dangling bonds of Cr atoms that near to X vacancy.[21,22] Interestingly, all the defect bands distribute in spin-up channel, which indicate a strong spin selectivity, and reduced the gap to 0.46, 0.35 and 0.15 eV for CrCl₃, CrBr₃ and CrI₃, respectively. This is different from the nonmagnetic 2D semiconductor MoS₂, in which the defect states induced by S vacancy is not spin-polarized.[23]

Perfect CrX₃/Gr

The atomic structures of CrI₃/Gr and CrCl₃/Gr (CrBr₃/Gr) heterostructures are sketched in Figure 3(a) and (b). Firstly, we try to determine the most stable stacking configuration by comparing the total energies of various heterostructures obtained by sliding CrX₃ layer along zigzag and armchair directions. However, the total energies difference is tiny. Hence the interactions between CrX₃ and graphene do not exhibit evident site selectivity, which is in line with reports about of CrI₃/Gr, CrBr₃/Gr and RuCl₃/Gr heterostructures.[19,20,24] Nevertheless, in our previous study, we found the strong site-dependence of total energies in CrX₃/silicene and CrX₃/germanene heterostructures.[25] The difference may be originated from the bulking of silicene and germanene. The interlayer distances *d* are measured to be about 3.36, 3.45 and 3.47 Å for CrCl₃/Gr, CrBr₃/Gr and CrI₃/Gr, respectively. These distances are much large than the sum of covalent atomic radii of C and X, indicating there are no chemical bonds between C and X atoms, and the interlayer interactions are dominated by van der Waals force. However, the interlayer distances are larger than the distances in CrX₃/metal heterostructures.[26] To evaluate the interlayer interaction strength, we calculated the interlayer binding energy *E_b* by

$$E_b = (E_{Gr} + E_{CrX_3} - E_{tot})/A \quad (1)$$

where *E_{Gr}*, *E_{CrX₃}* and *E_{tot}* are the total energies of isolated graphene, CrX₃ and CrX₃/Gr

heterostructures, respectively. A is the area of the interface. The calculated E_b for CrCl₃/Gr, CrBr₃/Gr and CrI₃/Gr are 9.68, 17.38 and 14.34 meV/Å², respectively. The results are consistent with previous studies,[19,20] also comparable to the 18.4 meV/Å² of GaSe/Gr heterostructures.[27] However, the binding energies between CrX₃ and graphene are much smaller than the binding energies, about 1 J/m² (62.5 meV/Å²), between CrX₃ and metal surfaces at the same level.[26] The very different interlayer binding energies in CrX₃/Gr and CrX₃/metal heterostructures is easy to understand. The graphene is dangling-bond free, while redundant electrons may be hosted by metal surface, which may participate in the bonds between CrX₃ and the metal surface.

To further evaluate the interlayer interaction, we calculate the charge density difference (CDD) of CrX₃/Gr heterostructures, which is defined by

$$\Delta\rho = \rho(heterostructure) - \rho(graphene) - \rho(CrX_3) \quad (2)$$

Similar features can be found in the results, so we representatively show the result of CrBr₃/Gr in Fig 3(c) and (d). As we can see, the charge depletion occurs at the graphene layer with charge accumulation at Br atoms of CrBr₃ positioned close to graphene, and there is no charge redistribution at the outside Br atoms. Interestingly, we also observe a small amount of charge accumulation at Cr atoms. This result indicates graphene is a charge-donating substrate for CrX₃, and it is expectable as the calculated work function of graphene (4.28 eV) is smaller than the electron affinity of CrX₃ (5.38, 4.73, and 4.69 eV for CrCl₃, CrBr₃ and CrI₃, respectively). This is different to the MoS₂/Gr heterostructure, in which the charge transfers from MoS₂ to graphene.[28] The interlayer charge transfer can give rise to a built-in electric field points from graphene layer to CrX₃. Our result identifies with experimental result that the CrI₃ is n-doped when contact with graphene.[29] Moreover, previous studies have proved that charge doping can effectively tune the magnetic properties of CrX₃. [25,30,31] Therefore, the interlayer charge transfer may be one way to tune the magnetic properties of CrX₃ in CrX₃/Gr heterostructures. Besides, in the experimental study of Mak et. al,[32] the observed magnetic circular dichroism signal of BN/CrI₃/Gr and BN/CrI₃/BN systems show significant difference. For comparison, we also study the CrI₃/BN heterostructure, and find the charge transfer between CrI₃ and BN layer is much less than that between CrI₃ and graphene. Therefore, the different magnetic properties of BN/CrI₃/Gr and BN/CrI₃/BN systems may be originated from the different charge transfer and built-in electric field in CrI₃/Gr and CrI₃/BN interfaces. Afterwards, we quantificationally calculate the transferred charge Δq per CrX₃ unit by Bader charge analysis.[33] The results are 0.072, 0.015 and 0.003 e for CrCl₃/Gr, CrBr₃/Gr and CrI₃/Gr, which are in line with the order of electron affinities of CrX₃.

The projected density of states (PDOS) are calculated to reveal the electronic properties of CrX₃/Gr, and we present the PDOS of CrBr₃/Gr in Fig 4. In single-layer CrX₃, the d orbitals of Cr atom split into triple degenerate t_{2g} orbit and double degenerate e_g orbit. However, the PDOS demonstrates the partial breaking of degeneracy of d states in CrX₃/Gr. For example, the d_{z^2} orbit is no longer degenerate with $d_{x^2-y^2}$ orbit. This is due to the broken inversion symmetry and formation of z-direction built-in electric field.

Therefore, the vdW engineering provides an effective way to tune the orbital characteristic of 2D materials. However, the orbits of CrX3 retain partial degeneracy, such as the d_{xy} and d_{xz} orbits, and different from the complete breaking in CrX3/metal heterostructures.[26] By carefully structural checking, we find the atomic structure of CrX3 in heterostructure is almost the same as single-layer, which is in contrast with great deformation when CrX3 interacts with metal surface.[26] Fig 4(d) depicts the PDOS of graphene. The states near Fermi level are disturbed to some extent, indicating weak hybridization between graphene and CrX3. In addition, the states of spin-up and spin-down direction are no longer symmetric. Therefore, net magnetic moments are induced in graphene due to the magnetic proximity effect, which will break the time reversal symmetry in graphene, and may bring about quantum phase transition.[19,20]

Next, we calculate the spin-polarized band structures of the CrX3/Gr heterostructures. The band structures of these three systems show similar features, so we show the band of CrBr3/Gr in Fig 5. We can see that the Dirac cone of graphene is well preserved, confirming the vdW interaction. It is similar to the graphene on nonmagnetic semiconductor GaSe and MoS2.[27,28] However, the Dirac cone moves upward and submerge into the conduction band, consisting with the result that charge transfers from graphene to CrX3. Our results are very similar to the reports,[19,20] but different from Klein's result,[10] in which there is a certain amount of states distributed across Fermi level. This difference possibly comes from the different layers of graphene and CrI3 in supercell that used in calculation. To visualize the real-space distribution of bottom of conduction bands in spin-up and spin-down direction, we plot the partial charge density. Due to the dense and flat bands, the charge densities of four bands at the bottom of conduction band in each spin direction are evaluated. The results are shown in Fig 5(d) and (e). We can be informed that the charge mainly distributes around the Cr atoms in both spin directions. It indicates the transport process in both spin directions is principally involved by the d states of Cr atoms. However, the spin-down partial charge density extents widely than spin-up, and there is more charge distributes around X atoms. Interestingly, there is a small quantity of p_z orbital charge distributed at graphene.

To reveal the energy level alignment, and illustrate the effects of interlayer interactions on band structures of CrX3, we project the band of heterostructures to CrX3 layer in spin-up and spin-down direction. Fig 5(b) and (c) depict the projected bands of CrBr3 layer. We find the band structures of CrX3 in heterostructure are very similar to single-layer. For example, the gaps in spin-up and spin-down direction of CrBr3 layer in heterostructure are 1.34 and 2.42 eV, which are very close to the 1.36 and 2.57 eV of single-layer CrBr3. Therefore, the electronic properties of CrX3 are influenced slightly by the interlayer interactions. This is similar to the case of GaSe/Gr heterostructure, where the change of GaSe layer gap is only about 0.01 eV by the interlayer interaction.[27]

Now we turn to the contact properties of CrX3/Gr, as the electronic transport through the interface between CrX3 and graphene is an interesting topic now. When electron

transports through metal-semiconductor interface, the barrier it encountered may be composed by two parts, namely tunneling barrier (Φ_{TB}) and Schottky barrier (Φ).^{34,35} In vdW metal-semiconductor interface, because the the large vdW gap and weak interlayer orbital hybridization, the Φ_{TB} may be pronounced. To evaluate the tunneling barrier height, we calculate the effective electrostatic potential along Z-direction (V_{eff}). Fig 6(a) depict the V_{eff} of CrBr3/Gr, and illustrates the definition of Φ_{TB} , which is the potential difference between the vdW gap and CrX3 layer. The calculated Φ_{TB} are 7.0, 6.5 and 5.4 eV for CrX3/Gr (X=Cl, Br and I). The values are larger than the case of MoS2/metal interfaces, in which Φ_{TB} is smaller than 1 eV.[36]

Afterwards, we try to evaluate the Schottky barrier (Φ). As experiments mainly probe the electrons tunneling process, we merely consider the Schottky barrier height for electron, Φ_e . Interestingly, due to the exchange splitting in magnetic semiconductor, the electrons with different spin direction will exhibit different transport properties. Therefore, according to Schottky-Mott rule,[37] the barrier heights for spin-up/down electrons $\Phi_{e_up/dn}$ can be defined as

$$\Phi_{e_up/dn} = E_{CBM_up/dn} - E_F \quad (3)$$

where E_F is the Fermi energy, $E_{CBM_up/dn}$ is the energy of conduction band minimum (CBM) in spin-up/down direction of CrX3 in the heterostructure. The measured values are listed in Table 2. The values of Φ_e for spin-up are much less than for spin-down. For instance, in CrBr3/Gr, the Φ_{e_up} is 61 meV, while Φ_{e_dn} is as large as 547 meV. As the tunneling barrier is Coulomb interaction nature and does not exhibit spin selectively, the different Φ_{e_up} and Φ_{e_dn} signify different barriers will be encountered by spin-up and spin-down electrons when they transport through the interface. The spin-dependent barriers will give rise to different tunneling rates for spin-up and spin-down electrons, thus generate spin-filter effect. This is consistent with the remarkable spin-filter effect observed by experiments. [10,11,29] Kim et. al[14,15] have studied the electronic transport barrier based on devices composed by bilayer CrX3 and few layers graphene, they found the barrier height is spin-dependent, such as CrBr3, the height is 477 meV and 599 meV for spin-up and down-electron. Our result is qualitatively consistent with the report. However, big discrepancy exists among the values. There are several reasons may account for the divergence. Firstly, under different bias and temperature, electrons transport across the metal-semiconductor may be dominated by different mechanisms.[38] The barrier height extracted by Kim et. al is based on Fowler-Nordheim tunneling under high bias at low temperature 1.4 K. However, the Schottky barrier play a dominant role in Schottky emission under low bias and higher temperature.[39] Secondly, the GGA-PBE functional is well-known for imprecise estimation of band gap. Thirdly, the different material layers used in experiment and our calculation.

The introduction of X vacancy

We further study the properties of CrX3/Gr with one X vacancy, denoted by CrX3/Gr@Xv. Structurally, the X vacancy can be distributed inside (V_{in}) and outside

(V_{out}) in heterostructure, as shown in Figure 7(a). To determine the stable configuration, we calculate the binding energy E_b for V_{in} and V_{out} configurations, as shown in Figure 7(b). In all these hybrid systems, the E_b for V_{out} is larger than V_{in} , suggesting the X vacancies are inclined to distribute at V_{out} site in these heterostructures. However, the X vacancies show slight effects on E_b . In CrCl₃/Gr, the Cl vacancy enhances the interlayer binding slightly for both V_{in} and V_{out} , similar to the enhancement of interlayer binding caused by intrinsic atomic vacancies in BN/Gr and MoSe₂/metal heterostructures.[40,41] While in CrBr₃/Gr and CrI₃/Gr, the interlayer binding will be weakened by Br(I) vacancy, especially the vacancy distributed at V_{in} . The X vacancy has competitive effects on the interlayer binding. On one hand, the vacancy results in dangling bonds, which can increase the interlayer charge transfer, and lead to positive contribution to E_b . On the other hand, X atom is the acting point of vdW interaction, thus the missing of X will reduce the interlayer binding. Then, as the distance between graphene and inside X atom is smaller than outside X atom, the missing of inside X atom has more negative influence on interlayer interaction than outside X atom. Therefore, the E_b for V_{out} is larger than V_{in} . Furthermore, as the vdW interaction is positive correlated with atomic numbers, the missing of heavier atom leads to greater loss of vdW interaction. As competitive results, the Cl vacancy increases E_b , while Br (I) decreases E_b .

Next, we calculate the band structures of the CrX₃/Gr with atomic vacancy. Despite the different atomic structure and interlayer binding energy for V_{in} and V_{out} configurations, the band structures seem to be structural insensitive. Therefore, we present the band structures of the systems at the energetically favorable V_{out} configuration in Fig 8. The Dirac cone of graphene is well preserved, the same as the perfect heterostructures. However, we can observe obvious interactions between the defect bands and π band of graphene. Such as CrI₃/Gr, the defect bands are fractured markedly by interaction.

Finally, we plot the projected band of CrX₃ layer in spin-up and down direction, as shown in Fig 8. The spin-down bands are very similar to the bands of perfect heterostructures, except for the positions of band edges. For example, the band edges of CrI₃ layer in spin-down direction are -1.12 and 1.05 eV, moving up about 0.2 eV relative to the -1.35 eV and 0.76 eV in perfect CrI₃/Gr. The difference in band edges can mainly be attributed to the n-doping by X vacancy. More interestingly, in spin-up direction, the Fermi level crosses the spin-up band of CrX₃ layer, it suggests the Ohmic contact in spin-up direction in CrX₃/Gr. The formation of spin-up direction Ohmic contact is due to the spin-selective defect band induced by X vacancy and interlayer charge transfer. It will enhance the transport of spin-up electrons, and then the SF effect, and may even inject current to graphene with 100% spin-polarization. In addition, the tunneling barriers Φ_{TB} in CrX₃/Gr@Xv are 6.5, 6.09 and 5.08 eV, reduced by about 0.4 eV comparing to the perfect ones. Hence, the X vacancy can entirely enhance conductivity of the interface.

Conclusion

In summary, a systematic study has been conducted to the CrX₃/Gr vdW heterostructures. The results show the charge transfer from graphene and leading to n-doping in CrX₃. Due to the unique band structures of CrX₃, the Schottky barriers in heterostructures for electrons Φ_e demonstrate strong spin-dependence, which may result in SF effect and be responsible for the observed large TMR values. In addition, upon the introduction of X vacancy, spin-selective Ohmic contacts form in CrX₃/Gr with the reduced tunneling barrier. Therefore, the defect-engineering may be an effective way to tune the spintronics properties of magnetic vdW heterostructures.

Calculation method

All our spin-polarized density functional calculations are carried out using the Vienna ab initio simulation package (VASP).[42,43] The ion-electron interactions are described by projected augmented wave (PAW) method with cutoff energy of 500 eV.[44] The generalized gradient approximation is used to evaluate the exchange-correction.[45] DFT-D2 method proposed by Grimme[46] is adopted to account for the interlayer van der Waals interactions. A vacuum thickness of 18 Å is used to avoid the artificial interaction between images of slabs. The convergent criterion of electronic step is set to 1×10^{-5} eV and the ions will be relaxed until the forces acted on each ion is smaller than 1×10^{-2} eV/Å. Brillouin zone sampling is done by a $5 \times 5 \times 1$ Γ -center mesh.[47]

Acknowledgement

This work was supported by National Natural Science Foundation of China (Grant No.11847157 and No.11874092) the Fok Ying-Tong Education Foundation, China (Grant No. 161005), the Planned Science and Technology Project of Hunan Province (Grant No. 2017RS3034), Hunan Provincial Natural Science Foundation of China (Grant No. 2016JJ2001 and 2019JJ50636), and Scientific Research Fund of Hunan Provincial Education Department (Grant No. 16B002 and 18C0227)

References

- (1) Mermin, N. D.; Wagner, H. Absence of ferromagnetism or antiferromagnetism in one- or two-dimensional isotropic Heisenberg models. *Phys. Rev. Lett.* 1966, 17, 1133.
- (2) Huang, B.; Clark, G.; Navarro-Moratalla, E.; Klein, D. R.; Cheng, R.; Seyler, K. L.; Zhong, D.; Schmidgall, E.; McGuire, M. A.; Cobden, D. H.; Yao, W.; Xiao, D.; Jarillo Herrero, P.; Xu, X. Layer-dependent ferromagnetism in a van der Waals crystal down to the monolayer limit. *Nature* 2017, 546, 270.
- (3) Pershoguba, S. S.; Banerjee, S.; Lashley, J. C.; Park, J.; Agren, H.; Aeppli, G.; Balatsky, A. V. Dirac Magnons in Honeycomb Ferromagnets. *Phys. Rev. X* 2018, 8, 011010.
- (4) Ghazaryan, D.; Greenaway, M. T.; Wang, Z.; Guarochico-Moreira, V. H.; VeraMarun, I. J.; Yin, J.; Liao, Y.; Morozov, S. V.; Kristanovski, O.; Lichtenstein, A. I., et al. Magnon-assisted tunnelling in van der Waals heterostructures based on CrBr₃.

- Nat. Elect.* 2018, 1, 344.
- (5) Zutic, I.; Fabian, J.; Sarma, S. D. Spintronics: Fundamentals and applications. *Rev. Mod. Phys.* 2004, 76, 323.
- (6) Moodera, J. S.; Santos, T. S.; Nagahama, T. The phenomena of spin-filter tunnelling. *J Phys.: Condens. Matter.* 2007, 19, 165202
- (7) Miao, G.-X.; Münzenberg, M.; Moodera, J. S. Tunneling path toward spintronics. *Rep. Prog. Phys.* 2011, 74, 036501.
- (8) Novoselov, K.; Mishchenko, A.; Carvalho, A.; Neto, A. C. 2D materials and van der Waals heterostructures. *Science* 2016, 353, aac9439.
- (9) Kim, H. H.; Yang, B.; Patel, T.; Sfigakis, F.; Li, C.; Tian, S.; Lei, H.; Tsen, A. W. One Million Percent Tunnel Magnetoresistance in a Magnetic van der Waals Heterostructure. *Nano Lett.* 2018, 18, 4885-4890.
- (10) Klein, D. R.; MacNeill, D.; Lado, J. L.; Soriano, D.; Navarro-Moratalla, E.; Watanabe, K.; Taniguchi, T.; Manni, S.; Canfield, P.; Fernández-Rossier, J., et al. Probing magnetism in 2D van der Waals crystalline insulators via electron tunneling. *Science* 2018, 360, 1218-1222.
- (11) Song, T.; Cai, X.; Tu, M. W.-Y.; Zhang, X.; Huang, B.; Wilson, N. P.; Seyler, K. L.; Zhu, L.; Taniguchi, T.; Watanabe, K., et al. Giant tunneling magnetoresistance in spin-filter van der Waals heterostructures. *Science* 2018, 360, 1214-1218.
- (12) Wang, Z.; Gutiérrez-Lezama, I.; Ubrig, N.; Kroner, M.; Gibertini, M.; Taniguchi, T.; Watanabe, K.; Imamoglu, A.; Giannini, E.; Morpurgo, A. F. Very large tunneling magnetoresistance in layered magnetic semiconductor CrI₃. *Nat. Commun.* 2018, 9, 2516.
- (13) Cai, X.; Song, T.; Wilson, N. P.; Clark, G.; He, M.; Zhang, X.; Taniguchi, T.; Watanabe, K.; Yao, W.; Xiao, D., et al. Atomically Thin CrCl₃: An in-Plane Layered Antiferromagnetic Insulator. *Nano Lett.* 2019,
- (14) Kim, H. H.; Yang, B.; Tian, S.; Li, C.; Miao, G.-X.; Lei, H.; Tsen, A. W. Tailored Tunnel Magnetoresistance Response in Three Ultrathin Chromium Trihalides. *Nano Lett.* 2019, 19, 5739-5745.
- (15) Kim, H. H.; Yang, B.; Li, S.; Jiang, S.; Jin, C.; Tao, Z.; Nichols, G.; Sfigakis, F.; Zhong, S.; Li, C., et al. Evolution of interlayer and intralayer magnetism in three atomically thin chromium trihalides. *Proc. Natl. Acad. Sci. U. S. A* 2019, 116, 11131-11136.
- (16) Zhang, W.-B.; Qu, Q.; Zhu, P.; Lam, C.-H. Robust intrinsic ferromagnetism and half semiconductivity in stable two-dimensional single-layer chromium trihalides. *J. Mater. Chem. C* 2015, 3, 12457-12468.
- (17) Lado, J. L.; Fernández-Rossier, J. On the origin of magnetic anisotropy in two dimensional CrI₃. *2D Mater.* 2017, 4, 035002.
- (18) Liu, J.; Sun, Q.; Kawazoe, Y.; Jena, P. Exfoliating biocompatible ferromagnetic Crtrihalide monolayers. *Phys. Chem. Chem. Phys.* 2016, 18, 8777-8784.
- (19) Zhang, J.; Zhao, B.; Zhou, T.; Xue, Y.; Ma, C.; Yang, Z. Strong magnetization and Chern insulators in compressed graphene/CrI₃ van der Waals heterostructures. *Phys. Rev. B: Condens. Matter. Mater. Phys.* 2018, 97, 085401.

- (20) Zhang, H.; Ning, Y.; Yang, W.; Zhang, J.; Zhang, R.; Xu, X. Possible realization of the high-temperature and multichannel quantum anomalous Hall effect in graphene/CrBr₃ heterostructures under pressure. *Phys. Chem. Chem. Phys.* 2019, 21, 17087-17095.
- (21) Zhao, Y.; Lin, L.; Zhou, Q.; Li, Y.; Yuan, S.; Chen, Q.; Dong, S.; Wang, J. Surface vacancy-induced switchable electric polarization and enhanced ferromagnetism in monolayer metal trihalides. *Nano Lett.* 2018, 18, 2943-2949.
- (22) Lin, C.; Li, Y.; Wei, Q.; Shen, Q.; Cheng, Y.; Huang, W. Enhanced Valley Splitting of Transition-Metal Dichalcogenide by Vacancies in Robust Ferromagnetic Insulating Chromium Trihalides. *ACS Appl. Mater. Inter.* 2019, 11, 18858-18864.
- (23) Li, H.; Huang, M.; Cao, G. Markedly different adsorption behaviors of gas molecules on defective monolayer MoS₂: a first-principles study. *Phys. Chem. Chem. Phys.* 2016, 18, 15110-15117.
- (24) Biswas, S.; Li, Y.; Winter, S. M.; Knolle, J.; Valentí, R. Electronic Properties of α -RuCl₃ in Proximity to Graphene. *Phys. Rev. Lett.* 2019, 123, 237201.
- (25) Li, H.; Xu, Y.-K.; Lai, K.; Zhang, W.-B. The Enhanced Ferromagnetism of Single-Layer CrX₃ (X= Br and I) by Van der Waals Engineering. *Phys. Chem. Chem. Phys.* 2019,
- (26) Pan, L.; Huang, L.; Zhong, M.; Jiang, X.-W.; Deng, H.-X.; Li, J.; Xia, J.-B.; Wei, Z. Large tunneling magnetoresistance in magnetic tunneling junctions based on twodimensional CrX₃ (X=Br, I) monolayers. *Nanoscale* 2018, 10, 22196-22202.
- (27) Si, C.; Lin, Z.; Zhou, J.; Sun, Z. Controllable Schottky barrier in GaSe/graphene heterostructure: the role of interface dipole. *2D Mater.* 2016, 4, 015027.
- (28) Pierucci, D.; Henck, H.; Avila, J.; Balan, A.; Naylor, C. H.; Patriarche, G.; Dappe, Y. J.; Silly, M. G.; Sirotti, F.; Johnson, A. C., et al. Band alignment and minigaps in monolayer MoS₂-graphene van der Waals heterostructures. *Nano Lett.* 2016, 16, 4054-4061.
- (29) Jiang, S.; Li, L.; Wang, Z.; Shan, J.; Mak, K. F. Spin tunnel field-effect transistors based on two-dimensional van der Waals heterostructures. *Nat. Elect.* 2019, 2, 159.
- (30) Wang, H.; Fan, F.; Zhu, S.; Wu, H. Doping enhanced ferromagnetism and induced half-metallicity in CrI₃ monolayer. *EPL-Europhys. Lett.* 2016, 114, 47001.
- (31) Zheng, F.; Zhao, J.; Liu, Z.; Li, M.; Zhou, M.; Zhang, S.; Zhang, P. Tunable spin states in the two-dimensional magnet CrI₃. *Nanoscale* 2018, 10, 14298-14303.
- (32) Jiang, S.; Shan, J.; Mak, K. F. Electric-field switching of two-dimensional van der Waals magnets. *Nat. Mater.* 2018, 17, 406.
- (33) Tang, W.; Sanville, E.; Henkelman, G. A grid-based Bader analysis algorithm without lattice bias. *J Phys.: Condens. Matter.* 2009, 21, 084204.
- (34) Allain, A.; Kang, J.; Banerjee, K.; Kis, A. Electrical contacts to two-dimensional semiconductors. *Nat. Mater.* 2015, 14, 1195.
- (35) Shen, T.; Ren, J.-C.; Liu, X.; Li, S.; Liu, W. van der Waals stacking induced transition from Schottky to ohmic contacts: 2D metals on multilayer InSe. *J Am. Chem. Soc.* 2019, 141, 3110-3115.
- (36) Popov, I.; Seifert, G.; Tománek, D. Designing electrical contacts to MoS₂ monolayers: a computational study. *Phys. Rev. Lett.* 2012, 108, 156802.

- (37) Tung, R. T. The physics and chemistry of the Schottky barrier height. *Appl. Phys. Rev.* 2014, 1, 011304.
- (38) Sze, S. M.; Ng, K. K. *Physics of semiconductor devices*; John Wiley & sons, 2006.
- (39) Liu, Y.; Guo, J.; Zhu, E.; Liao, L.; Lee, S.-J.; Ding, M.; Shakir, I.; Gambin, V.; Huang, Y.; Duan, X. Approaching the Schottky-Mott limit in van der Waals metal-semiconductor junctions. *Nature* 2018, 557, 696.
- (40) Park, S.; Park, C.; Kim, G. Interlayer coupling enhancement in graphene/hexagonal boron nitride heterostructures by intercalated defects or vacancies. *J Chem. Phys.* 2014, 140, 134706.
- (41) Huang, L.; Tao, L.; Gong, K.; Li, Y.; Dong, H.; Wei, Z.; Li, J. Role of defects in enhanced Fermi level pinning at interfaces between metals and transition metal dichalcogenides. *Phys. Rev. B: Condens. Matter. Mater. Phys.* 2017, 96, 205303.
- (42) Kresse, G.; Hafner, J. Ab initio molecular dynamics for liquid metals. *Phys. Rev. B: Condens. Matter. Mater. Phys.* 1993, 47, 558-561.
- (43) Kresse, G.; Furthmüller, J. Efficient iterative schemes for ab initio total-energy calculations using a plane-wave basis set. *Phys. Rev. B: Condens. Matter. Mater. Phys.* 1996, 54, 11169-11186.
- (44) Kresse, G.; Joubert, D. From ultrasoft pseudopotentials to the projector augmented-wave method. *Phys. Rev. B: Condens. Matter. Mater. Phys.* 1999, 59, 1758-1775.
- (45) Perdew, J. P.; Burke, K.; Ernzerhof, M. Generalized Gradient Approximation Made Simple. *Phys. Rev. Lett.* 1996, 77, 3865-3868.
- (46) Grimme, S. Semiempirical GGA-type density functional constructed with a long-range dispersion correction. *J Comput. Chem.* 2006, 27, 1787-1799.
- (47) Monkhorst, H. J.; Pack, J. D. Special points for Brillouin-zone integrations. *Phys. Rev. B: Condens. Matter. Mater. Phys.* 1976, 13, 5188-5192.

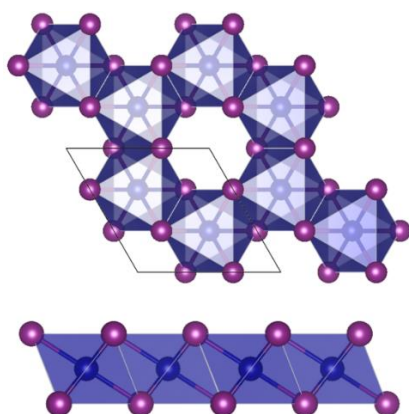


Figure 1 The top and side view of the atomic structure CrX₃. The blue and purple balls represent the Cr and X atoms.

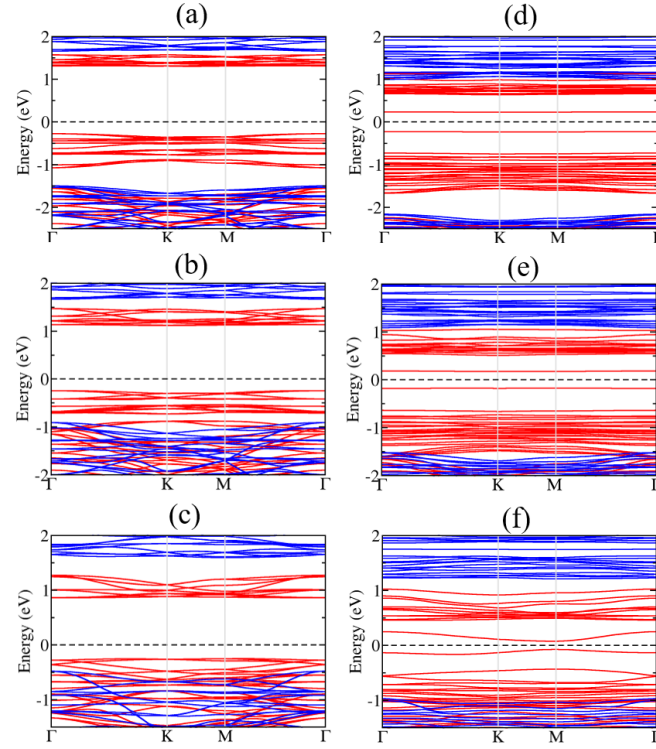


Figure 2 (a)(b) and (c) the spin-polarized band structure of pristine single-layer CrCl₃, CrBr₃ and CrI₃. (d)(e) and (f) the spin-polarized band structure of defective single-layer CrCl₃, CrBr₃ and CrI₃.

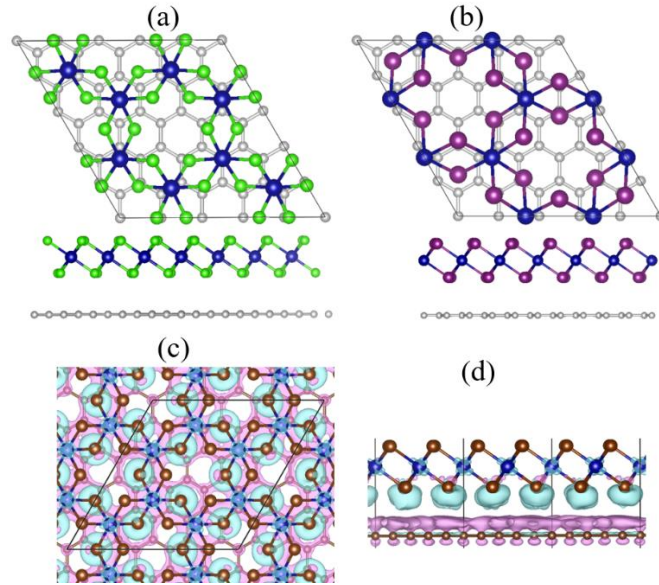


Figure 3 (a)(b) The atomic structure sketch of CrCl₃/Gr (CrBr₃/Gr) and CrI₃/Gr heterostructures. (c)(d) The top and side view of the charge density difference (CDD) of CrBr₃/Gr. The purple and blue denote the charge depletion and accumulation, and the isosurface is set to $0.0001 \text{ e}/\text{\AA}^3$

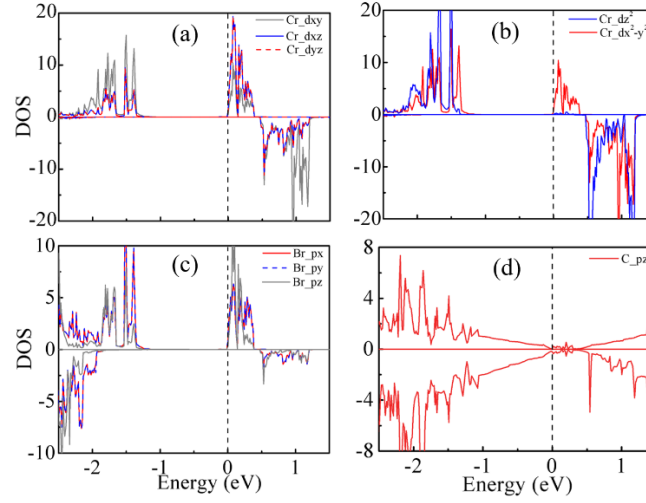


Figure 4 The projected density of states (PDOS) of (a)(b) the d orbitals of Cr atom, (c) the p orbitals of Br atom, (d) pz orbital of C atom. The Fermi level is set to zero.

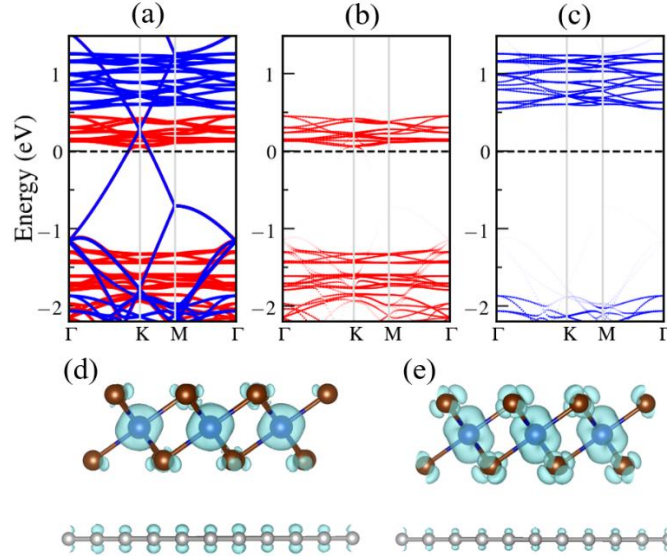


Figure 5 The spin-polarized band structure of CrBr₃/Gr, (a), the red and blue curves denote spin-up and down band. The projected band of CrBr₃ layer in CrBr₃/Gr heterostructure in spin-up, (b), and down spin-down, (c), direction. The partial charge density of the bottom of conduction band in spin-up, (d), and spin-down, (e), direction. The isosurface is set to 0.0025 e/Å³.

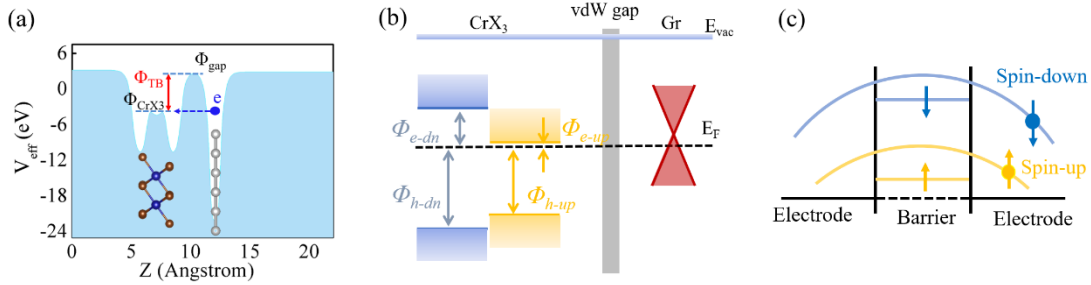


Figure 6 (a) Effective potential profile of CrBr₃/Gr interface, (b) Schematic drawings of the band alignments for the CrX₃/Gr heterostructures, (c) schematic energy diagram of barriers for spin-up and down electrons.

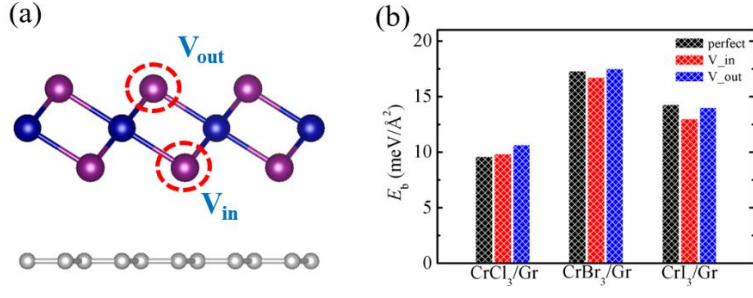


Figure 7 (a) Schematic drawing of two different configuration of defective heterostructures, (b) the binding energy E_b for perfect, V_{in} and V_{out} CrX₃/Gr heterostructures

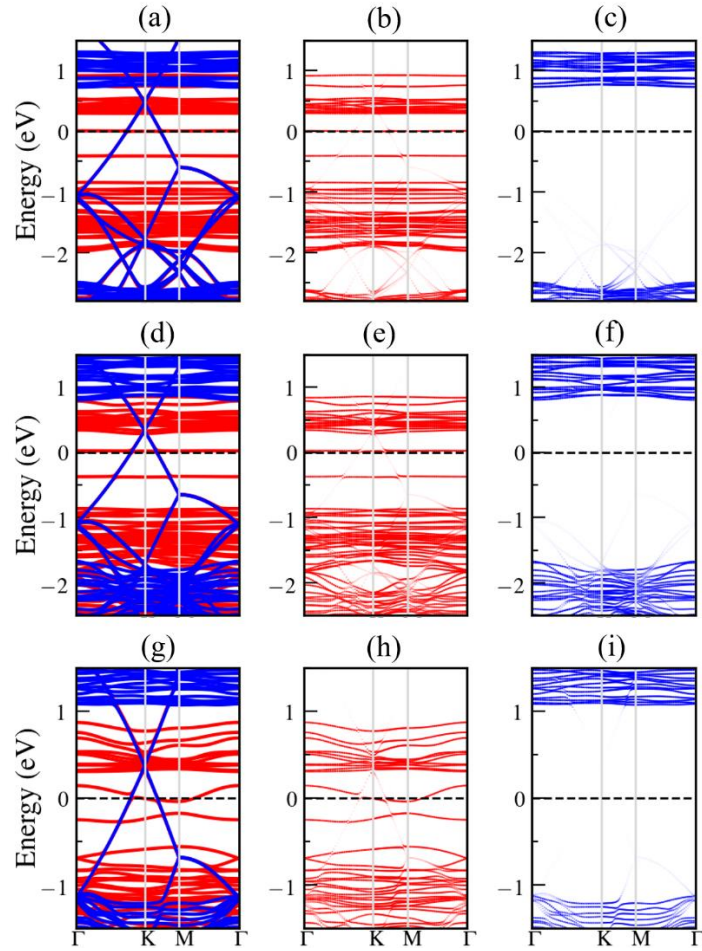


Figure 8 The spin-polarized band structure of defective (a) CrCl₃/Gr, (b) CrBr₃/Gr and (c) CrI₃/Gr. The projected band of (b)(c) CrCl₃, (e)(f) CrBr₃ and (h)(i) CrI₃ layer in spin-up and down direction in defective CrCl₃/Gr, CrBr₃/Gr and CrI₃/Gr heterostructure, respectively. The red and blue curves denote spin-up and down band.

Table 1 The calculated parameters in CrX3/Gr. d , interlayer distance, in Å; E_b , binding energy, in meV/Å²; Δq , transferred charge per CrX3 unit, in e.

| | CrCl3/Gr | CrBr3/Gr | CrI3/Gr |
|------------|----------|----------|---------|
| d | 3.36 | 3.45 | 3.47 |
| E_b | 3.36 | 17.38 | 14.34 |
| Δq | 0.072 | 0.015 | 0.003 |

Table 2 The Schottky barriers for electron Φ_e in spin-up, Φ_{e_up} , and spin-down, Φ_{e_dn} , in CrCl3/Gr, CrBr3/Gr and CrI3/Gr. The unit is meV.

| | Φ_{e_up} | Φ_{e_dn} |
|----------|----------------|----------------|
| CrCl3/Gr | 79 | 563 |
| CrBr3/Gr | 61 | 547 |
| CrI3/Gr | 34 | 759 |